

Effective modification of photocatalytic and piezocatalytic performances for poly(heptazine imide) by carbon dots decoration †

 Author and affiliation details can be edited in the panel that appears to the right when you click on the author list.

Shijie Wang^{a,†}, Haoqing Zhang^{a,†}, Ran Nie^a, Yuxin Ning^a, Chenxi Zhao^a, Zhonghui Xia^a, Ping Niu,^{(ID 0000-0002-4781-3098)^{a,*}}, Li Li,^{(ID 0000-0003-2308-916X)^a} and Shulan Wang,^{(ID 0000-0003-0098-5682)^b}

^aSchool of Metallurgy, Northeastern University, Shenyang 110819, P. R. China, niup@smm.neu.edu.cn

^bDepartment of Chemistry, College of Science, Northeastern University, Shenyang 110819, Liaoning, P. R. China

[†]These authors contributed equally.

Funding Information

 We have combined the funding information you gave us on submission with the information in your acknowledgements. This will help ensure the funding information is as complete as possible and matches funders listed in the Crossref Funder Registry. Please check that the funder names and award numbers are correct. For more information on acknowledging funders, visit our website: <http://www.rsc.org/journals-books-databases/journal-authors-reviewers/author-responsibilities/#funding>.

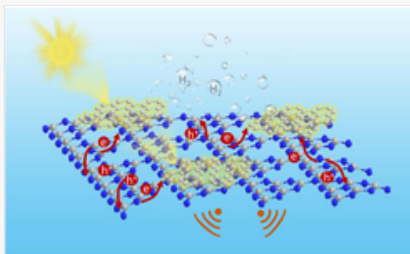
Funder Name :	National Natural Science Foundation of China
Funder's main country of origin :	
Funder ID :	10.13039/501100001809
Award/grant Number :	5190204551904059

Funder Name :	Fundamental Research Funds for the Central Universities
Funder's main country of origin :	
Funder ID :	10.13039/501100012226
Award/grant Number :	N2225038N182505036N2002005

Funder Name :	China Association for Science and Technology Young Elite Scientist Sponsorship Program by CAST (YESS)
Funder's main country of origin :	China
Funder ID :	10.13039/100010097
Award/grant Number :	2019-2021QNRC

Table of Contents Entry

Figure Replacement Requested



This work provides an effective strategy to modify the photocatalytic and piezoelectric catalytic activities of poly(heptazine imide) (PHI) by decorating with a low amount of carbon dots.

Replacement Image: TOC.jpg

Replacement Instruction: Replace image requested

Abstract

As the high-crystalline phase of carbon nitride, poly(heptazine imide) (PHI) has attracted much attention in recent years, considering [the its](#) more effective light absorption, better charge carrier behavior, and higher surface area of PHI compared with its counterpart with a melon structure that is commonly synthesized through thermal polymerization. Nevertheless, exploring effective strategies to further improve the performance of PHI is still highly desirable. In this work, it is revealed that the photocatalytic as well as piezocatalytic performances of PHI are greatly promoted by coupling with carbon dots (CDots) through a facile ultrasonication process. Detailed structure characterizations indicate that a very low content of CDots (0.05%) decoration can double the light absorbance and achieve the efficient separation and transfer of photogenerated charge carriers. The optimal photocatalytic hydrogen evolution rate of PHI/CDots is about 2.49 and 2.81 times that of PHI, under UV-Visible and visible light irradiation, respectively. Moreover, the piezocatalytic H₂O₂ generation and KMnO₄ degradation activities of PHI/CDots are around 2 times that of PHI. The results obtained in this work provide references for the modification of PHI and may inspire new strategies for the design of highly efficient carbonaceous photocatalysts.

Introduction

Photocatalysis is of great significance for a sustainable and green society, which can avoid the problematic issues caused by burning fossil fuels. Developing applicable photocatalysts with high efficiency, facile production, low cost, and high stability is the fundamental issue in promoting the application of photocatalysis technology in the industry. Among the various photocatalysts reported, graphitic carbon nitride (GCN) has attracted overwhelming attention since its discovery as a photocatalyst in 2009, and it has emerged as the “holy grail” photocatalyst in recent years, in addition to its variable applications in the fields of fuel cells, energy storage, electrocatalysis, *etc.*¹⁻⁶ Previously, the most widely investigated GCN has been obtained by direct polymerization of nitrogen-rich precursors (such as cyanamide, urea, dicyandiamide, melamine, *etc.*), which generally have the melon structure.^{1,7-9} Despite its merits of proper band position, variable modulation, facile synthesis, and low cost, the insufficient absorption and the high recombination rate of charge carriers greatly limited the photocatalytic activities.¹⁰ In the past, different strategies have been explored to modify the light absorption properties and charge carrier behavior of melon, with a special focus on defects control (such as intrinsic structural defects of vacancies and cyano groups,^{8,11,12} heteroatom doping,¹³⁻¹⁵ *etc.*), morphology modulation¹⁶⁻¹⁸ and composite construction.^{19,20}

Besides these investigations, in recent years, much attention has been aroused for the counterpart materials called poly(triazine imide) (PTI) and poly(heptazine imide) (PHI), which are synthesized by metal salt assisted processes.²¹ Compared with melon, which has the in-plane structure composed of strands of [hydrogen-bonded heptazine rings polymeric units](#) with the hydrogen bonds existing between the strands,²² the PTI and PHI are supposed to have a completing condensation with the formation of more intimately cohered triazine imide or heptazine imide, attributing to the effective roles of metal salts.²³⁻²⁵ As a result, the PTI and PHI can have better charge carrier transfer properties than melon.^{23,26} Especially, contrary to the blue shifted light absorption of PTI,²³ the PHI has extended light

absorption properties than melon. Combining with the merit of larger surface area, the PHI structure was reported to have much higher (even orders of magnitude) photocatalytic activities than melon and PTI.²⁶ Recently, the pioneer works indicate that due to the asymmetric triangular holes in the structure, GCN can have piezocatalytic activities.^{27,28} Interestingly, the PHI was also found to have better piezocatalytic activities than Melon.²⁹ However, related research is still in its infancy. To develop more possibilities for PHI, exploring new strategies is quite desirable.

Constructing composites has been widely reported to be effective in modifying photocatalytic performances through utilizing the advantages as well as creating the synergistic effect of the composing materials.³⁰⁻³² In this aspect, introducing new materials without destroying the structure of PHI while reinforcing the advantages of PHI is necessary. Among various materials, carbon materials with sp^2 configuration (such as graphene, carbon nanotubes, fullerene, carbon dots, *etc.*) are supposed to be good counterpart materials to provide transfer channels and restrict the recombination of charge carriers by π - π interactions.³³⁻³⁶ Especially, carbon dots (CDots) with ultrasmall sizes have extraordinary advantages, such as good dispersion and unique up-conversion properties.³⁷ Previously, CDots decoration has shown great potential in improving the photocatalysis and (photo-)piezocatalysis performances, working as photosensitizers, charge carrier transfer promoters or catalysts.³⁶⁻⁴⁰ For example, the CDots decorated melon structure C_3N_4 showed benchmark overall water splitting activities (solar-to-hydrogen efficiency of 2.0%, robust stability in 200 runs). In the C_3N_4 /CDots composite, CDots contributed to the improved visible light absorption and catalyzed the two-step reaction for O_2 evolution.³⁸ Besides, it was reported that the (photo-)piezocatalytic H_2O_2 generation performances of $BaTiO_3:Nb$ (Nb-doped tetragonal $BaTiO_3$) can be significantly improved by the modification of carbon quantum dots, which not only worked as the sensitizer but also promoted the charge transfer on the surface.⁴⁰ More attempts on the CDots modified photocatalysts and piezocatalysts are widely desirable.

In this work, we constructed PHI/CDots composites by a simple ultrasonication process without additional thermal treatment, and the PHI/CDots composite with a very low content of Cdots (0.05%) shows obviously increased activities than PHI not only in the photocatalytic RhB degradation and water splitting reactions but also in the piezocatalytic H_2O_2 generation and $KMnO_4$ degradation reactions. By structural characterizations and photoelectrochemical tests, the roles of carbon dots were studied.

Experimental section

Materials

Melamine ($C_3H_6N_6$) was purchased from Sinopharm Chemical Reagent Co., Ltd. Potassium chloride (KCl) and sodium chloride (NaCl) were purchased from Tianjin Yongda Chemical Reagent Co., Ltd. Lithium chloride (LiCl) and carbon quantum dots (CDots) were purchased from Shanghai Macklin Biochemical Technology Co., Ltd. All chemicals were of analytical grade and were used without further purification. The water used in the experiments was deionized water.

Preparation of photocatalysts

Bulk carbon nitride was synthesized by thermal condensation of melamine. Typically, 20 g of melamine was placed in a covered ceramic crucible and was calcined in a muffle furnace at 550 °C for 4 h. After grinding, a yellow powder was obtained and denoted as CN.

Poly(heptazine imide) (PHI) was synthesized as follows: 1 g of CN was ground with 5.1 g KCl, 5.1 g NaCl, and 4.8 g LiCl in a mortar. The mixture was calcined at 550 °C for 4 h under N_2 atmosphere. To remove the residual chloride salts, the product was washed with deionized water thoroughly and dried in an oven at 60 °C overnight. The obtained product is denoted as PHI.

PHI/CDots was synthesized by ultrasonication process. In detail, 50 ml suspension with 0.1 g PHI and different contents of CDots (2 mg L^{-1} , 5/25/50 mL) was ultrasonicated (KQ-200VDE, Kunshan ultrasonic instrument) for 2 h at constant temperature (20 °C). After drying in an oven at 60 °C, the samples were denoted as PHI/CDots- x , where x represents the volume of carbon quantum dots. The PHI treated under a similar process without the addition of CDots was named PHI-U.

Microstructural characterizations

X-ray diffraction (XRD) characterization was carried out on D8 Discover (Brook, USA) using Cu K α rays for radiation. Fourier transform infrared spectroscopy (FT-IR) was conducted using an IS20 analog Fourier transform infrared spectrometer (FT-IR, Thermo Fisher Scientific). Scanning electron microscopy (SEM) and transmission electron microscopy (TEM) images were collected on SU8010 (Tianmei Co., Ltd) and TECNAI G2 F30 S-TWIN (FEI, US). UV-Vis absorption spectra were obtained on a JACSCO-500 spectrophotometer. Steady-state fluorescence spectra were measured on a fully functional steady-state fluorescence spectrometer, Fluoromax-4 (Horiba, Japan), under the excitation of 350 nm. X-ray photoelectron spectroscopy (XPS) was conducted on Thermo ESCALAB 250XI with monochromatic AlK α radiation, and the binding energy was calibrated using the C 1s peak at 284.8 eV as standard.

Photocatalytic reactions

The photocatalytic Rhodamine B (RhB) degradation tests were conducted as follows: 25 mg powder sample was added to 80 mL RhB solution with the concentration of 20 mg L⁻¹. After dark adsorption for 30 min, the suspension was irradiated by a 300 W Xe lamp ($\lambda > 300$ nm). The visible light irradiation ($\lambda > 420$ nm) was realized by using a cutoff filter. At certain time intervals, 5 mL of the suspension was collected and centrifuged. The absorbance at $\lambda = 554$ nm was recorded for the supernatant using a UV-Vis spectrophotometer. To identify the active species in the photocatalytic RhB degradation reaction, similar processes were performed under visible light irradiation ($\lambda > 420$ nm), except for the different scavengers including triethanolamine (TEOA), isopropanol (IPA), and benzoquinone (BQ) were added to trap h⁺, [•]OH, and [•]O₂⁻, respectively.

The photocatalytic hydrogen evolution activity tests were executed as follows: 100 mg sample as well as 3 wt% Pt was added to 100 mL of triethanolamine (TEOA) solution (TEOA : water volume ratio = 1 : 9). The quartz reactor containing the above suspension was irradiated in a closed gas circulation system. UV-Visible light irradiation was conducted using a Xe lamp (Beijing Perfect Light Technology Co., Ltd, Microsolar 300), while visible light irradiation ($\lambda > 420$ nm) was realized using a cutoff filter. The amount of evolved hydrogen at different time intervals was quantified using gas chromatography (Tianmei, GC7900).

Photoelectrochemical tests

The photoelectrochemical tests were performed using a three-electrode system. Pt plate was used as the counter electrode, Ag/AgCl was used as the reference electrode, and 0.5 M Na₂SO₄ aqueous solution was used as the electrolyte. The FTO glass (2 cm × 1 cm) was used as the substrate after ultrasonic cleaning with acetone, ethanol, and deionized water sequentially. Then, the slurry obtained by dispersing the powder sample and PVDF (mass ratio of 9 : 1) in *N*-methylpyrrolidone was coated on FTO (1 cm² coating area) as the working electrode. The photocurrent curves (*I*-*t*) and the electrochemical impedance spectroscopy (EIS) were tested using the CHI660D electrochemical workstation. The photocurrent tests were carried out at 0.3 V under a Xenon lamp (300 W) with a cutoff filter ($\lambda > 420$ nm) as the visible light source. For the EIS test, the potential was set to the open circuit voltage, and the frequency was set to 0.01–100 000 Hz.

Piezocatalytic reactions

The piezocatalytic reduction of KMnO₄ was carried out as follows. 100 mg of the sample was added to 100 mL of KMnO₄ solution (40 mg L⁻¹). The suspension was stirred for 30 min to reach the adsorption equilibrium (in the dark). Then, the suspension was reacted under simultaneous stirring and ultrasonication in the dark (in a 45 kHz ultrasonic cleaner combined with an electric stirrer). 5 mL of the sample solution was taken out every 30 min. After filtration, the concentration of KMnO₄ was determined by measuring the absorbance peak at 525 nm in a spectrophotometer.

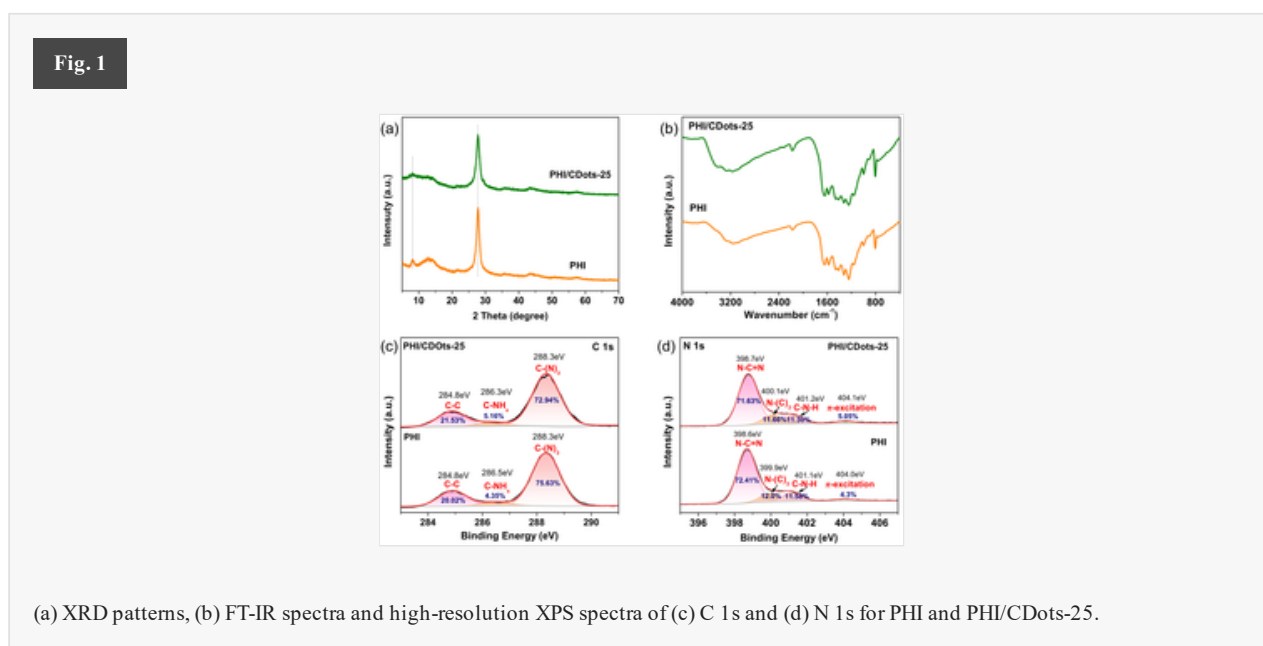
The piezocatalytic H₂O₂ generation was carried out as follows. 50 mg of sample was added to 100 mL of water. The solution was reacted under continuous stirring and sonication conditions in the dark. 3 mL of the sample solution was taken out every 30 min, and the amount of generated H₂O₂ was measured with a UV-Vis spectrophotometer. Firstly, the indicator solution was prepared by dissolving 0.25 g of bi-*o*-toluidine in 90 mL of acetic acid and then diluting the solution to 100 mL. 2 mL of the supernatant reaction solution was mixed with 0.5 mL of the indicator. After the

reaction, 2 mL of 1 mol L⁻¹ hydrochloric acid was added for further acidification. The concentration of H₂O₂ was determined by measuring the absorbance at 436 nm with a UV-Vis spectrophotometer.

Results and discussion

Atomic structure and morphology characterizations

The PHI was obtained by metal salt-assisted treatment of melon and the PHI/CDots composites were synthesized through facile ultrasonic processes with varied amounts of CDots. As indicated by the XRD patterns (Fig. S1[†]), the melon obtained by direct polymerization of melamine has two main peaks at 12.9° and 27.1°, reflecting the periodic diffraction of the in-plane arrangement and the layer stacking of GCN, respectively.¹ Comparatively, treating melon at 550 °C with the assistance of metal salt has obviously changed the crystal structure (Fig. 1a). Firstly, the characteristic peak representing the layer stacking has a narrower full width at half maximum (FWHM) and shifted from 27.0° to 27.7° (Table S1[†]), indicating the higher crystallinity as well as the much denser packing of the interlayer structure. Such change is beneficial for the charge carrier migration between the layers.^{41,42} Secondly, a new peak appeared at 8.1°, reflecting the enlarged periodic arrangement, which is the characteristic peak for PHI originating from the more conjugated structure or the emergence of a new facet during the metal salt treatment.^{26,43} These results confirm that the PHI structure has been successfully obtained. After loading carbon dots on PHI by ultrasonication, the PHI/CDots show similar XRD patterns to PHI, indicating that CDots decoration did not influence the crystal structure during the mild synthesis process, and the absence of new peaks is attributed to the very low content of CDots. The PHI/CDots composites constructed by loading different contents of CDots have a similar crystal structure (Fig. S2[†]).

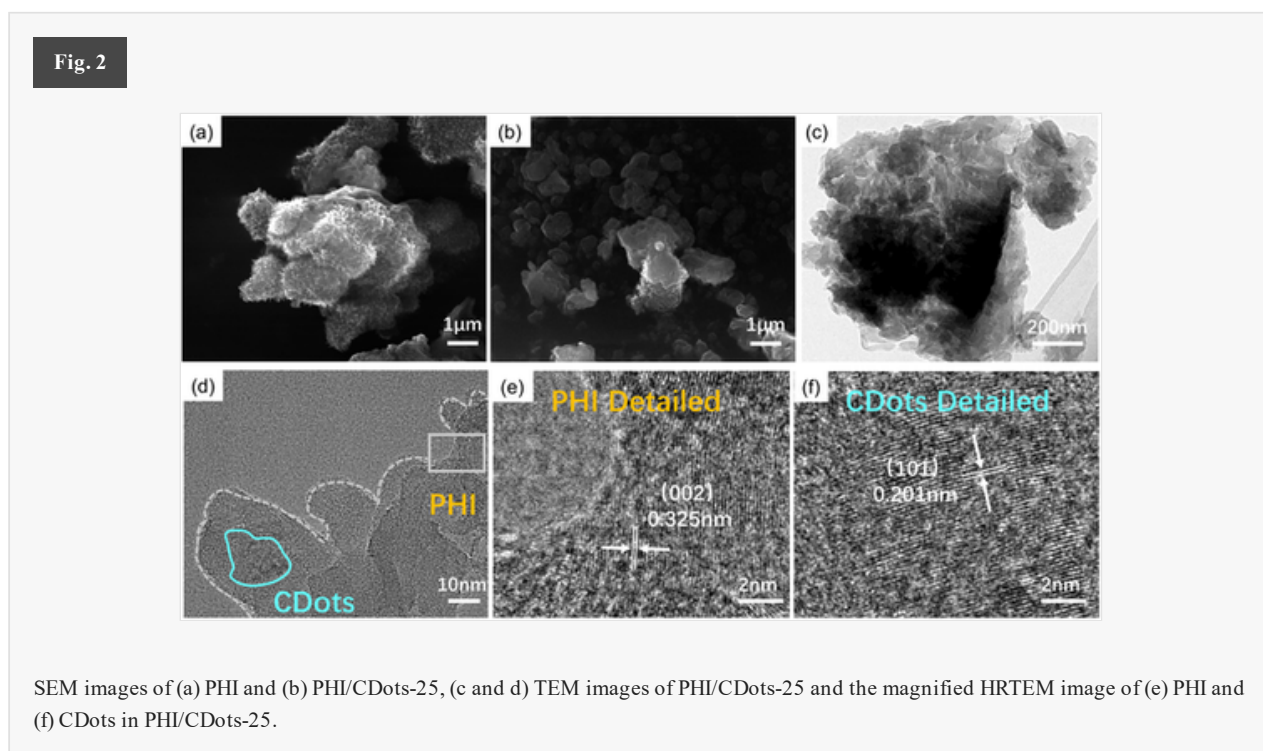


(a) XRD patterns, (b) FT-IR spectra and high-resolution XPS spectra of (c) C 1s and (d) N 1s for PHI and PHI/CDots-25.

The functional groups of PHI and PHI/CDots-25 were evaluated by FT-IR characterization. As shown in Fig. 1b, both PHI and PHI/CDots-25 show the FT-IR vibration of typical functional groups for graphitic carbon nitride.^{22,26,43,44} In detail, the peaks at 806 cm⁻¹ and 2165 cm⁻¹ represent the bending vibration of the heptazine ring and the cyano groups, respectively.^{22,43} The peaks between 900–1700 cm⁻¹ correspond to the characteristic vibration of the heptazine structure,^{22,26} while the broad peaks between 3000–3500 cm⁻¹ indicate the existence of NH/NH₂ and OH/H₂O groups.^{45–47} The PHI and PHI/CDots-25 show similar characteristic peaks in the FT-IR spectra, indicating that the deposition of CDots maintains the fundamental structure of PHI. The chemical states of PHI and PHI/CDots-25 were further characterized by XPS. As shown in Fig. S3,[†] the full spectrum of PHI and PHI/CDots-25 both have obvious peaks, reflecting the existence of C, N, O, and K. Note that the existence of K on the surface structure is consistent with the previous report.²⁶ The characteristic chemical environment of C and N is studied in detail. It is clear that the C 1s spectrum of PHI can be deconvoluted to three binding states of C–C, C–NH_x, and C(N)₃ while the N 1s spectrum can be deconvoluted to four binding states of C–N–C, N–(C)₃, C–N–H, and π excitation (Fig. 1c and d).^{48–50} Comparatively, the binding states of PHI/CDots-25 did not show a significant difference compared to PHI.

However, it is noted that upon the decoration of CDots, the C–C ratio in PHI/CDots is higher than PHI. Besides, the π excitation in N 1s increased for PHI/CDots, indicating the possible interaction between PHI and CDots.

The typical morphology of the synthesized PHI and PHI/CDots was characterized by scanning electron microscopy (SEM) and transmission electron microscopy (TEM). As shown in Fig. S4,[†] the melon obtained by direct polymerization of melamine shows thick flake morphology. Comparatively, the PHI shows porous morphology with the formation of some curly texture during the recondensation process (Fig. 2a), which is consistent with the previous literature.⁵¹ The PHI/CDots-25 has similar morphology to PHI (Fig. 2b), and the TEM image of PHI/CDots-25 indicates that the microstructure consists of stacked PHI nanoflakes with the carbon dots dispersed on the nanoflakes (Fig. 2c and d). The lattice spacing of 0.325 nm was observed in the high resolution TEM image (Fig. 2e and Fig. S5[†]), representing the stacking distance between layers in the PHI structure. Meanwhile, the lattice spacing of 0.981 nm is also observed (Fig. S6[†]), reflecting the intra-plane periodic arrangement, which is consistent with the diffraction peak at 8.1° in the XRD patterns. These results further evidenced the formation of the PHI structure. Besides, the lattice spacing of 0.201 nm was observed (Fig. 2f), which corresponds to the (101) facet of CDots. The co-existence of PHI and CDots indicates the successful synthesis of PHI/CDots composites.

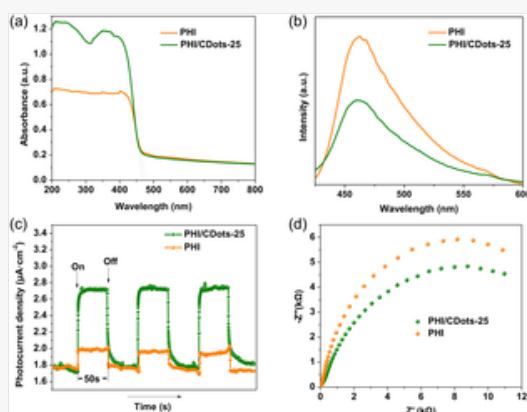


Analysis of band structure and behaviour of charge carriers

The above results show that CDots have been successfully loaded on PHI. To study the influence of CDots decoration on the physical properties of PHI, UV-Vis diffuse reflectance spectroscopy was firstly recorded. As shown in Fig. 3a, the light absorption edges of PHI and PHI/CDots-25 are 478 nm and 467 nm, respectively, with the bandgap of PHI and PHI/CDots-25 determined to be 2.582-65 and 2.652-58 eV, respectively (Fig. S7[†]). Besides the slightly decreased/modified bandgap, interestingly, the light absorbance of PHI/CDots-25 has significantly increased (almost double) compared with PHI. Previous investigation has shown that the strong contact and interaction in the heterostructure can lead to high light absorption coefficient and the CDots loading can effectively improve the light harvesting properties.⁵²⁻⁵⁴ Thus, it is assumed that the strong interaction between PHI and CDots results in the obviously increased light absorbance, which is beneficial for the photocatalytic efficiency of PHI/CDots if the photogenerated charge carriers can be effectively utilized. Thus, to acknowledge the subsequent charge carrier behavior, photoluminescence (PL) spectroscopy as well as electrochemical tests were conducted. The PL spectra (Fig. 3b) show that the PHI/CDots-25 has a similar emission peak to PHI, but the intensity of PHI/CDots-25 is obviously lower than PHI. The lower PL intensity indicates the surface charge recombination has been mitigated, possibly due to the charge carrier sink effect of CDots,⁵⁵ which promotes efficient interfacial charge transfer between CDots and PHI, resulting in improved charge carrier separation and the decreased charge carrier recombination.⁵⁶⁻⁵⁸ Moreover, the PHI/CDots-25 shows a much higher transient photocurrent response ($1 \mu\text{A cm}^{-2}$) than PHI ($0.3 \mu\text{A cm}^{-2}$), as shown

in Fig. 3c, indicating the promoted transfer of photogenerated electron-hole pairs.⁴⁰ PHI/CDots-25 has a smaller radius in the electrochemical impedance spectroscopy (EIS) Nyquist plots compared with PHI (Fig. 3d), reflecting the better transport and lower transfer resistance of charge carriers by CDots decoration.^{40,42}

Fig. 3

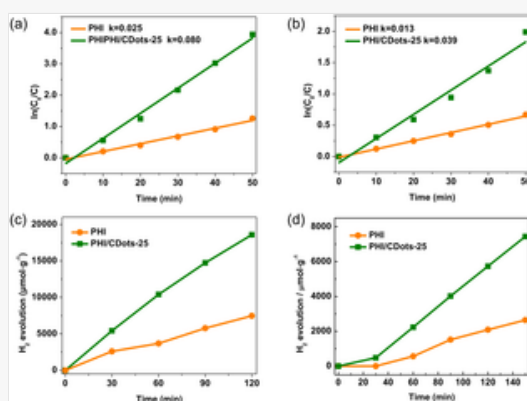


(a) UV-Vis diffuse reflectance spectra, (b) photoluminescence (PL) emission spectra, (c) transient photocurrent density-time plots, and (d) electrochemical impedance spectroscopy (EIS) Nyquist plots of PHI and PHI/CDots-25.

Evaluation of photocatalytic and piezocatalytic activities

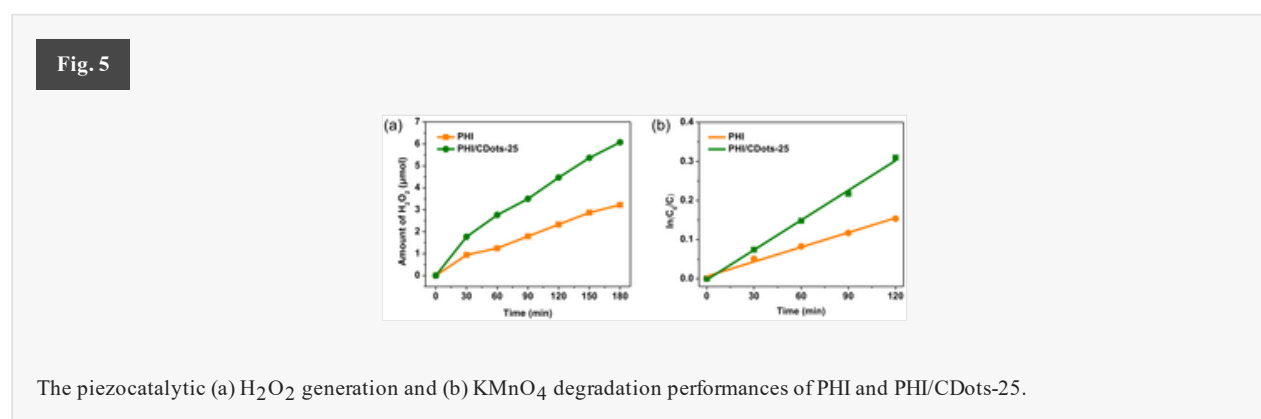
The above results show that under light irradiation, not only more electron-hole pairs can be generated in PHI/CDots, but also the recombination of electron-hole pairs can be retarded due to the transfer between PHI and CDots. The photocatalytic activities were then evaluated by RhB degradation and hydrogen evolution from water splitting. As shown in Fig. S8,[†] the photocatalytic RhB degradation for PHI is higher than that for Melon, indicating the superiority of PHI. The PHI/CDots with different amounts of CDots have obviously higher photocatalytic activity than PHI, and the PHI/CDots-25 show the optimal performance. Moreover, the photocatalytic RhB degradation for PHI and PHI/CDots-25 follows pseudo-first order kinetics, and the rate constant value for PHI/CDots-25 is 3.2 and 3 times that of PHI under UV-Visible light irradiation and visible light irradiation, respectively (Fig. 4a and b). The pure CDots show no photocatalytic activity and the PHI-U has similar photocatalytic activity with PHI (Fig. S9[†]), indicating the synergistic effect between PHI and CDots is crucial for the excellent performance of PHI/CDots-25. The active species generated and utilized in the photocatalytic RhB degradation reactions were investigated by adding different scavengers, triethanolamine (TEOA), isopropanol (IPA), and benzoquinone (BQ) to trap h^+ , $\cdot OH$, and $\cdot O_2^-$ respectively. It is noted that both for PHI (Fig. S10[†]) and PHI/CDots-25 (Fig. S11[†]), the three scavengers can obviously decrease the degradation efficiency, indicating the h^+ , $\cdot OH$, and $\cdot O_2^-$ are all generated under visible light irradiation and have played important roles in the degradation of RhB. Comparatively, the h^+ and $\cdot O_2^-$ are more effective for the degradation of RhB than $\cdot OH$ for both PHI and PHI/CDots. Moreover, the stronger influence of scavengers on PHI/CDots than PHI evidences the more effective generation and utilization of active species in PHI/CDots.

Fig. 4



The photocatalytic hydrogen evolution from water splitting was evaluated further. It is noted that the PHI has much higher photocatalytic hydrogen evolution rates than Melon (Fig. S12–S14[†]), which further supports the superiority of the PHI structure. More importantly, the PHI/CDots-25 has hydrogen evolution rates of 9293 and 2975 $\mu\text{mol g}^{-1} \text{h}^{-1}$ under UV-Visible and visible light irradiation, which is 2.49 and 2.81 times that of PHI, respectively (Fig. 4c and d). The photocatalytic performances clearly show that with a small amount of CDots loading, the photocatalytic activities of PHI can be obviously increased. According to the structural and physicochemical analysis, the decoration of CDots can effectively modify the photocatalytic processes by improving the light absorption properties as well as promoting the transfer and separation of charge carriers, which results in the much higher photocatalytic activities of PHI/CDots composites. Moreover, the quite stable hydrogen evolution performance of PHI/CDots-25 is viewed (Fig. S15[†]).

Considering the effective modification of charge carrier behavior by CDots decoration, the piezocatalytic performances of the samples were further evaluated. As indicated, the piezocatalytic activities of H_2O_2 generation (Fig. 5a) and KMnO_4 degradation (Fig. 5b) for PHI/CDots-25 are about two times that for PHI, indicating the effectiveness of CDots decoration for promoting the piezocatalytic processes, while pure CDots did not show obvious piezoelectric activities (Fig. S16[†]). As reported, the polarized charge transfer is important for piezocatalysis, and the facilitation of free charge transfer can promote piezocatalytic performances.⁴⁰ It is assumed that the promoted separation, the smoother transfer, and utilization of charge carriers in PHI/CDots also play important roles in the piezocatalytic processes and thus increase the efficiency of the piezocatalytic reactions.



Conclusions

In summary, carbon dots (CDots) and poly(heptazine imide) were integrated through a facile ultrasonication process. Due to the strong interaction between CDots, the PHI/CDots presented greatly increased absorbance as well as significantly improved separation and transfer of charge carriers. Accordingly, the PHI/CDots shows obviously enhanced photocatalytic and piezocatalytic activities compared to PHI. This work provides a valuable reference for the deep insight of PHI and promotes the development of carbonaceous materials in photocatalysis and piezocatalysis.

Author contributions

Shijie Wang: Methodology, experiment, data collation. Haoqing Zhang: Methodology, experiment, data collation. Ran Nie: Experiment, data collation. Yuxin Ning: Data collation. Chenxi Zhao: Data collation. Zhonghui Xia: Data collation. Ping Niu: Conceptualization, methodology, funding acquisition, writing – review & editing. Li Li: Methodology, writing – review & editing. Shulan Wang: Funding acquisition, writing – review & editing.

Conflicts of interest

There are no conflicts to declare.

Acknowledgements

We express our great thanks to the National Natural Science Foundation of China (51902045, 51904059), Fundamental Research Funds for the Central Universities (N2225038, N182505036, N2002005) and Young Elite



References can be edited in the panel that appears to the right when you click on a reference.

- 1 X. C. Wang, K. Maeda, A. Thomas, K. Takanaabe, G. Xin, J. M. Carlsson, K. Domen and M. Antonietti, *Nat. Mater.*, 2009, **8**, 76–80.
- 2 G. F. Liao, Y. Gong, L. Zhang, H. Y. Gao, G. J. Yang and B. Z. Fang, *Energy Environ. Sci.*, 2019, **12**, 2080–2147.
- 3 Y. Zheng, J. Liu, J. Liang, M. Jaroniec and S. Z. Qiao, *Energy Environ. Sci.*, 2012, **5**, 6717–6731.
- 4 F. K. Kessler, Y. Zheng, D. Schwarz, C. Merschjann, W. Schnick, X. C. Wang and M. J. Bojdys, *Nat. Rev. Mater.*, 2017, **2**, 17030.
- 5 P. Niu, J. J. Dai, X. J. Zhi, Z. H. Xia, S. L. Wang and L. Li, *InfoMat*, 2021, **3**, 931–961.
- 6 H. Wang, X. Liu, P. Niu, S. L. Wang, J. Shi and L. Li, *Matter*, 2020, **2**, 1377–1413.
- 7 J. H. Liu, Y. W. Zhang, L. H. Lu, G. Wu and W. Chen, *Chem. Commun.*, 2012, **48**, 8826–8828.
- 8 P. Niu, G. Liu and H. M. Cheng, *J. Phys. Chem. C*, 2012, **116**, 11013–11018.
- 9 S. C. Yan, Z. S. Li and Z. G. Zou, *Langmuir*, 2009, **25**, 10397–10401.
- 10 Y. Wang, X. C. Wang and M. Antonietti, *Angew. Chem., Int. Ed.*, 2012, **51**, 68–89.
- 11 P. Niu, M. Qiao, Y. Li, L. Huang and T. Y. Zhai, *Nano Energy*, 2018, **44**, 73–81.
- 12 J. Ding, W. Xu, H. Wan, D. S. Yuan, C. Chen, L. Wang, G. F. Guan and W. L. Dai, *Appl. Catal., B*, 2018, **221**, 626–634.
- 13 S. Guo, Z. Deng, M. Li, B. Jiang, C. Tian, Q. Pan and H. Fu, *Angew. Chem., Int. Ed.*, 2016, **55**, 1862–1866.
- 14 G. Liu, P. Niu, C. H. Sun, S. C. Smith, Z. G. Chen, G. Q. Lu and H. M. Cheng, *J. Am. Chem. Soc.*, 2010, **132**, 11642–11648.
- 15 Z. X. Qin, Z. X. Huang, M. L. Wang, D. Y. Liu, Y. B. Chen and L. J. Guo, *Appl. Catal., B*, 2020, **261**, 118211.
- 16 Y. P. Zhu, T. Z. Ren and Z. Y. Yuan, *ACS Appl. Mater. Interfaces*, 2015, **7**, 16850–16856.
- 17 X. H. Li, J. S. Zhang, X. F. Chen, A. Fischer, A. Thomas, M. Antonietti and X. C. Wang, *Chem. Mater.*, 2011, **23**, 4344–4348.
- 18 P. Niu, L. L. Zhang, G. Liu and H. M. Cheng, *Adv. Funct. Mater.*, 2012, **22**, 4763–4770.
- 19 Z. M. Pan, G. G. Zhang and X. C. Wang, *Angew. Chem.*, 2019, **131**, 7176–7180.
- 20 X. J. Chen, J. Wang, Y. Q. Chai, Z. J. Zhang and Y. F. Zhu, *Adv. Mater.*, 2021, **33**, e2007479.
- 21 L. H. Lin, Z. Y. Yu and X. C. Wang, *Angew. Chem.*, 2019, **131**, 6225–6236.

- 22 B. V. Lotsch, M. Doblinger, J. Sehnert, L. Seyfarth, J. Senker, O. Oeckler and W. Schnick, *Chem. – Eur. J.*, 2007, **13**, 4969–4980.
- 23 L. H. Lin, C. Wang, W. Ren, H. H. Ou, Y. F. Zhang and X. C. Wang, *Chem. Sci.*, 2017, 5506–5511.
- 24 L. H. Lin, Z. Y. Lin, J. Zhang, X. Cai, W. Lin, Z. Y. Yu and X. C. Wang, *Nat. Catal.*, 2020, 649–655.
- 25 A. Savateev, N. V. Tarakina, V. Strauss, T. Hussain, K. Brummelhuis, J. M. Sanchez Vadiillo, Y. Markushyna, S. Mazzanti, A. P. Tyutyunnik, R. Walczak, M. Oschatz, D. M. Guldi, A. Karton and M. Antonietti, *Angew. Chem., Int. Ed.*, 2020, **59**, 15061–15068.
- 26 L. H. Lin, H. H. Ou, Y. F. Zhang and X. C. Wang, *ACS Catal.*, 2016, **6**, 3921–3931.
- 27 M. Zelisko, Y. Hanlumyung, S. B. Yang, Y. M. Liu, C. H. Lei, J. Y. Li, P. M. Ajayan and P. Sharma, *Nat. Commun.*, 2014, **5**, 4284.
- 28 K. F. Wang, D. K. Shao, L. Zhang, Y. Y. Zhou, H. P. Wang and W. Z. Wang, *J. Mater. Chem.*, 2019, **7**, 20383–20389.
- 29 T. T. Xu, Z. H. Xia, H. G. Li, P. Niu, S. L. Wang and L. Li, *Energy Environ. Mater.*, 2022, DOI: 10.1002/eem2.12306.
- 30 M. Tayyab, Y. J. Liu, S. X. Min, R. Muhammad Irfan, Q. H. Zhu, L. Zhou, J. Y. Lei and J. L. Zhang, *Chin. J. Catal.*, 2022, **43**, 1165–1175.
- 31 X. J. Zhi, H. Liu, Z. H. Xia, S. L. Di, Y. Beom Cho, P. Niu, S. E. Chun, S. L. Wang and L. Li, *Sol. RRL*, 2022, **6**, 2100901.
- 32 T. T. Xu, P. Niu, S. L. Wang and L. Li, *J. Mater. Sci. Technol.*, 2021, **74**, 128–135.
- 33 L. Ge and C. C. Han, *Appl. Catal., B*, 2012, **117–118**, 268–274.
- 34 X. Chen, K. J. Deng, P. Zhou and Z. H. Zhang, *ChemSusChem*, 2018, **11**, 2444–2452.
- 35 Y. J. Zhang, T. Mori, L. Niu and J. H. Ye, *Energy Environ. Sci.*, 2011, **4**, 4517–4521.
- 36 B. Li, W. Peng, J. Zhang, J. C. Lian, T. Huang, N. Cheng, Z. Y. Luo, W. Q. Huang, W. Y. Hu, A. L. Pan, L. Jiang and G. F. Huang, *Adv. Funct. Mater.*, 2021, **31**, 2100816.
- 37 H. Zhang, L. X. Zhao, F. L. Geng, L. H. Guo, B. Wan and Y. Yang, *Appl. Catal., B*, 2016, **180**, 656–662.
- 38 J. Liu, Y. Liu, N. Y. Liu, Y. Z. Han, X. Zhang, H. Huang, Y. Lifshitz, S. T. Lee, J. Zhong and Z. H. Kang, *Science*, 2015, **347**, 970–974.
- 39 X. F. Zhou, B. Shen, A. Lyubartsev, J. W. Zhai and N. Hedin, *Nano Energy*, 2022, **96**, 107141.
- 40 X. F. Zhou, F. Yan, A. Lyubartsev, B. Shen, J. W. Zhai, J. C. Conesa and N. Hedin, *Adv. Sci.*, 2022, **9**, e2105792.
- 41 C. Merschjann, S. Tschierlei, T. Tyborski, K. Kailasam, S. Orthmann, D. Hollmann, T. Schedel-Niedrig, A. Thomas and S. Lochbrunner, *Adv. Mater.*, 2015, **27**, 7993–7999.
- 42 G. G. Zhang, G. S. Li, Z. A. Lan, L. H. Lin, A. Savateev, T. Heil, S. Zafeirotos, X. C. Wang and M. Antonietti, *Angew. Chem., Int. Ed.*, 2017, **56**, 1–6.

- 43 G. Q. Zhang, Y. S. Xu, C. X. He, P. X. Zhang and H. W. Mi, *Appl. Catal., B*, 2021, **283**, 119636.
- 44 Y. Li, F. Gong, Q. Zhou, X. H. Feng, J. J. Fan and Q. J. Xiang, *Appl. Catal., B*, 2020, **268**, 118381.
- 45 G. G. Liu, G. X. Zhao, W. Zhou, Y. Y. Liu, H. Pang, H. B. Zhang, D. Hao, X. G. Meng, P. Li, T. Kako and J. Ye, *Adv. Funct. Mater.*, 2016, **26**, 6822–6829.
- 46 Y. X. Wang, H. Wang, F. Y. Chen, F. Cao, X. H. Zhao, S. G. Meng and Y. J. Cui, *Appl. Catal., B*, 2017, **206**, 417–425.
- 47 P. He, X. Tang, L. Chen, P. Xie, L. He, H. Zhou, D. Zhang and T. Fan, *Adv. Funct. Mater.*, 2018, **28**, 1801121.
- 48 J. Li, B. Shen, Z. Hong, B. Lin, B. Gao and Y. Chen, *Chem. Commun.*, 2012, **48**, 12017–12019.
- 49 A. Thomas, A. Fischer, F. Goettmann, M. Antonietti, J.-O. Muller, R. Schlogl and J. M. Carlsson, *J. Mater. Chem.*, 2008, **18**, 4893–4908.
- 50 D. J. Martin, K. Qiu, S. A. Shevlin, A. D. Handoko, X. Chen, Z. Guo and J. Tang, *Angew. Chem., Int. Ed.*, 2014, **53**, 9240–9245.
- 51 Z. Zeng, H. Yu, X. Quan, S. Chen and S. Zhang, *Appl. Catal., B*, 2018, **227**, 153–160.
- 52 S. L. Shinde, S. Ishii, T. D. Dao, R. P. Sugavaneshwar, T. Takei, K. K. Nanda and T. Nagao, *ACS Appl. Mater. Interfaces*, 2018, **10**, 2460–2468.
- 53 D. Yang, G. Yang, S. Gai, F. He, C. Li and P. Yang, *ACS Appl. Mater. Interfaces*, 2017, **9**, 6829–6838.
- 54 Y. Liu, Y. Zhao, Y. Sun, J. Cao, H. Wang, X. Wang, H. Huang, M. Shao, Y. Liu and Z. Kang, *Appl. Catal., B*, 2020, **270**, 118875.
- 55 L. Ai, R. Shi, J. Yang, K. Zhang, T. Zhang and S. Lu, *Small*, 2021, **17**, e2007523.
- 56 X. Zhou, F. Yan, S. Wu, B. Shen, H. Zeng and J. Zhai, *Small*, 2020, **16**, e2001573.
- 57 X. Zhou, B. Shen, J. Zhai and N. Hedin, *Adv. Funct. Mater.*, 2021, **31**, 2009594.
- 58 Y. Wang, R. Godin, J. R. Durrant and J. Tang, *Angew. Chem., Int. Ed.*, 2021, **60**, 20811–20816.

Footnotes

[†] Electronic supplementary information (ESI) available. See DOI: <https://doi.org/10.1039/d2dt01819e>[[Instruction: In the given URL, we could not trace the supporting information of this work. Would please the editors confirm the information of the supplementary material we submitted? If there is any problem, please contact us.](#)]

Queries and Answers

Q1

Query: Funder details have been incorporated in the funder table using information provided in the article text. Please check that the funder information in the table is correct and indicate any changes, if required. If changes are required, please ensure that you also amend the Acknowledgements text as appropriate.

Answer: The mistaken funder information is revised.

Q2

Query: For your information: You can cite this article before you receive notification of the page numbers by using the following format: (authors), Dalton Trans., (year), DOI: 10.1039/d2dt01819e.

Answer: Thanks for the information.

Q3

Query: Have all of the author names been spelled and formatted correctly? Names will be indexed and cited as shown on the proof, so these must be correct. No late corrections can be made.

Answer: Yes, the author names are correct.

Q4

Query: Have all of the funders of your work been fully and accurately acknowledged? If not, please ensure you make appropriate changes to the Acknowledgements text.

Answer: Yes

Q5

Query: Ref. 29: Can this reference be updated? If so, please provide the relevant information such as year, volume and page or article numbers as appropriate.

Answer: The volume and page information of this reference has not been given on the internet.